

Structure and Magnetic Behavior of Cu^{II} MOFs Supported by 1,2,4-Triazolyl-Bifunctionalized Adamantane Scaffold

Ganna A. Senchyk,^[a] Andrey B. Lysenko,^{*[a]} Eduard B. Rusanov,^[b]
Alexander N. Chernega,^[b] Julia Jezierska,^[c] Konstantin V. Domasevitch,^[a] and
Andrew Ozarowski^{*[d]}

Keywords: Metal–organic frameworks / N ligands / Copper / EPR spectroscopy / Magnetic properties

New triazole-based Cu^{II} metal–organic frameworks, [Cu(tr₂ad)(SO₄)]·3H₂O (**1**), [Cu₃(tr₂ad)₄(H₂O)₂(SO₄)₂]SO₄·28H₂O (**2**), [Cu₃(tr₂ad)₄(H₂O)₄](SiF₆)₃·16H₂O (**3**), constructed utilizing a rigid adamantane scaffold, tr₂ad = 1,3-bis(1,2,4-triazol-4-yl)adamantane, were prepared hydrothermally, and their crystal structures were determined. The structure of **1** is built up from straight chains of corner-sharing CuN₄O₂ octahedra supported by short μ₂-tr (tr = 1,2,4-triazole) and μ₂-SO₄²⁻ bridges. The tetradentate character of tr₂ad results in the formation of layers. The 2D structures of **2** and **3** consist of discrete secondary building blocks [Cu₃(μ₂-Nⁱ,N^j-tr)₆] with triple [–N–N–] triazole links between the adjacent Cu centers [the Cu–(tr)–Cu separations are 3.806 and 3.756 Å for **2** and **3**, respectively]. The distorted octahedral N₄O₂ environment

of the peripheral Cu atoms is completed by water molecules and/or terminal sulfate anions. The linear magnetic clusters, which act as nodes, are joined together at average distances of 11.2 and 15.0–15.6 Å into square-grid-like networks that exploit the double-bridging μ₃- and μ₄-bis(triazole) modules. Uncoordinated counteranions and crystal water molecules fill the interlayer space and channels in the complexes and form extensive H-bonding patterns. The exchange integrals $J_1 = 9.8$ and $J_2 \approx 0$ cm⁻¹ for the interaction $J_1(\hat{S}_1\hat{S}_2 + \hat{S}_2\hat{S}_3) + J_2\hat{S}_1\hat{S}_3$ were determined for **3** from magnetic susceptibility data and reproduced by a broken-symmetry DFT calculation. The spin Hamiltonian parameters of **3** were found from high-field electron paramagnetic resonance (EPR) spectra.

Introduction

The remarkable coordination properties of 1,2,4-triazole ligands (tr) provide an enormous structural variety in their complexes^[1] (a few hundred crystal structures have been deposited with the Cambridge Crystallographic Data Center), which are built upon oligonuclear coordination clusters and may find diverse applications in the area of multifunctional magnetic materials.^[2,3] Among this ligand family, the 4-substituted derivatives with a single 1,2,4-triazole function are very suitable for the production of a variety of cluster geometries ranging from discrete dimers [M₂(μ-Nⁱ,N^j-tr)₃],^[4] linear [M₃(μ-Nⁱ,N^j-tr)₆],^[5] or triangular [M₃(μ₃-OH)(μ-Nⁱ,N^j-tr)₃] trimers^[6] to polymeric chains [M(μ₂-OH)(μ-

Nⁱ,N^j-tr)₂],^[7] [M(μ-Nⁱ,N^j-tr)₃],^[8] rare double-decker {μ₆-Cl[M₃(μ₃-OH)(μ-Nⁱ,N^j-tr)₃]}^[9] and fascinating metallacrown-like [Cu₆(μ₂-OH)₆] motifs.^[10] Therefore, they are of potential interest for the development of nanosized molecular magnets, spin-crossover materials for molecular sensing, etc. The nature of magnetic ordering as well as the strength of magnetic coupling in the metal clusters depends upon many factors such as ground-state configuration, magnetic transmission through short organic/inorganic bridges, and effects of lattice topology.^[11] As summarized in Table 1, the magnetic exchange interaction is very sensitive to the architecture of the whole cluster, which can be “tuned” by utilizing triazoles and anionic coligands.^[5b,6b,7,8a,8b,9,10,12–15]

The use of bi- or multifunctional ligands significantly expands the molecular design scope and provides a straightforward strategy for the incorporation of magnetic metalloclusters into 2D and 3D metal–organic frameworks. The addition of nucleophilic anions (SO₄²⁻, Cl⁻, OH⁻) significantly impacts the preference for one of the two dominant structural motifs (Scheme 1).

In our previous work, we showed a general method for the design of Cu^{II}- and Cd^{II}-triazole metal–organic frameworks (MOFs) by exploiting the predictable coordination behavior of bis(triazoles). These complexes also contain large and rigid aromatic (Ph)^[16] or polyhedral aliphatic spacers like diamondoids (e.g., adamantane).^[17]

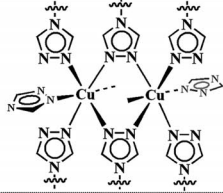
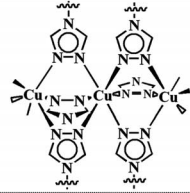
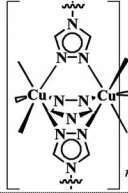
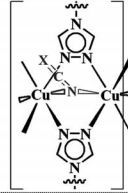
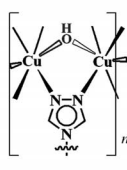
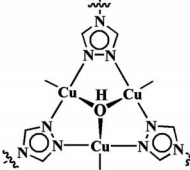
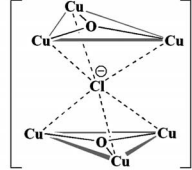
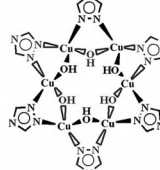
[a] Department of Inorganic Chemistry, Taras Shevchenko National University, Volodimirska Street 64, Kyiv 01033, Ukraine
Fax: +38-044-239-33-06
E-mail: ab_lysenko@univ.kiev.ua
Homepage: <http://inorganic.chem.univ.kiev.ua/ua/>

[b] Institute of Organic Chemistry, Murmanska Street 5, Kyiv 02660, Ukraine

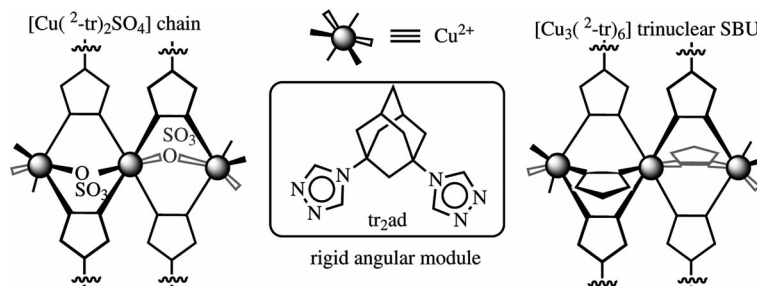
[c] Faculty of Chemistry, University of Wrocław, 14 Joliot-Curie Str., 50-383 Wrocław, Poland

[d] National High Magnetic Field Laboratory, Florida State University, 1800 E. Paul Dirac Drive, Tallahassee, FL 32310, USA
Supporting information for this article is available on the WWW under <http://dx.doi.org/10.1002/ejic.201200873>.

Table 1. Correlation of magnetic orderings and structural motifs in the Cu^{II}-1,2,4-tr complexes.

Cluster motifs; structural dimensionality				
	integrated dimers [Cu ₂ (N ⁱ ,N ^j -tr) ₂ (N ^k ,N ^l -tr) ₂]; 3D	[Cu ₃ (N ⁱ ,N ^j -tr) ₆]; molecular linear cluster	[Cu(N ⁱ ,N ^j -tr) ₃]; chain	[Cu(N ⁱ ,N ^j -tr) ₂ (μ-NCX) ₂], X = S, N; chain
1,2,4-Triazole ligands; counter anions	4,4'-bi(1,2,4-triazole); NO ₃ ⁻	2-(1,2,4-triazol-4-yl)pyridine; ClO ₄ ⁻	4-(2'-hydroxyethyl)-1,2,4-triazole; CF ₃ SO ₃ ⁻ , ClO ₄ ⁻	4-amino-1,2,4-triazole; NCS ⁻ , ClO ₄ ⁻ , N ₃ ⁻ , NO ₃ ⁻
$J^{[a]}$ [cm ⁻¹]	0.44 ^[b]	10.8 ^[b]	-1.45 ^[c] , 1.18 ^[c]	102 ^[b] , 35.4 ^[b]
Ref.	[12]	[56]	[8b,8a]	[13,14]
Cluster motifs; structural dimensionality				
	[Cu(μ ₂ -OH)(N ⁱ ,N ^j -tr)]; chain	(e) [Cu ₃ (μ ₃ -OH)(N ⁱ ,N ^j -tr) ₆ (NCS) ₃]; (f) [Cu ₃ (μ ₃ -OH)(N ⁱ ,N ^j -tr) ₃ A]; molecular triangular clusters	[Cu ₆ (μ ₆ -Cl)(μ ₃ -OH) ₂ (N ⁱ ,N ^j -tr) ₆ Cl ₆ (H ₂ O) ₃]; molecular double-decker complex	[Cu ₆ (μ ₂ -OH) ₆ (N ⁱ ,N ^j -tr) ₆]; cyclic molecular motif
1,2,4-Triazole ligands; counter anions	"Tr-Shiff bases"; BF ₄ ⁻ , NO ₃ ⁻ /OH ⁻	(e) 3,5-dimethyl-(1,2,4-triazol-4-yl)amine; (f) N-(4H-(1,2,4-triazol-3-yl)acetamide); (e) OH ⁻ /NCS ⁻ , ClO ₄ ⁻ (f) OH ⁻ /A = NO ₃ ⁻ , ClO ₄ ⁻ , CF ₃ SO ₃ ⁻	4-(1,2,4-triazol-4-yl)phenol; Cl ⁻ , OH ⁻	3,5-dimethyl-(1,2,4-triazol-4-yl)amine
$J^{[a]}$ [cm ⁻¹]	391-608 ^[c]	240 ^[b] , 190.9-198.2 ^[c]	102.8 ^[b]	AFM ^[d]
Ref.	[7]	[66,15]	[9]	[10]

[a] All J values refer to the Hamiltonian JS_iS_j and were converted as needed. A positive J indicates antiferromagnetic interaction. [b] Original paper used $-2JS_iS_j$. [c] Original paper used $-JS_iS_j$. [d] The experimental J value was not measured, ref.^[10]



Scheme 1. Two principal structural motifs in the MOFs studied in this paper.

Much attention has been paid to bi- or tetrafunctionalized adamantane-supported platforms, which were successfully utilized for the construction of related metal-carboxylate,^[18,19] metal-phosphonate,^[20] and Ag^I-sulfonate^[21] coordination polymers.

In this work, we describe the synthesis and crystal structures of three Cu^{II}-{1,3-bis(1,2,4-triazol-4-yl)adamantane} frameworks with incorporated trinuclear secondary building units (SBUs) or chain motifs and either tetrahedral SO₄²⁻ or octahedral SiF₆²⁻ counter dianions. The magnetic behavior of complex **3** is described and discussed on the basis of its structural features.

Results and Discussion

In general, tr₂ad typically acts as a μ₃- and/or a μ₄-donor ligand, which bridges the metal ions at remarkably short (3.3–3.8 Å) distances thanks to the ability of the 1,2,4-tri-

azole moieties to form –N–N– bridges. Very long (10.5 Å) distances may be achieved, on the other hand, when employing the adamantane spacer.^[17]

In the crystal structure of **1** (Figure 1a, Table 2), the Cu^{II} atoms are organized into columns of apical O,O-corner-sharing distorted Cu octahedra CuN₄O₂. The Cu1...Cu1 (3.532 Å) separations along the polymeric chains are supported by the cooperative interactions of μ₂-tr and μ₂-SO₄²⁻ anions. The tetradentate bis(triazole) ligands link two pairs of Cu^{II} atoms from the neighboring columns, which leads to further corrugated layers with narrow channels running along the b axis. The van der Waals cross-section of the channels (ca. 1 × 4 Å), is not large enough to accommodate solvent molecules.

The sulfate tetrahedra occupy two opposite axial positions in the coordination sphere (Cu1–O1 2.406 Å) and are oriented towards the interlayer space. Thus, the angular adamantane spacers form hydrophobic channel walls in the b

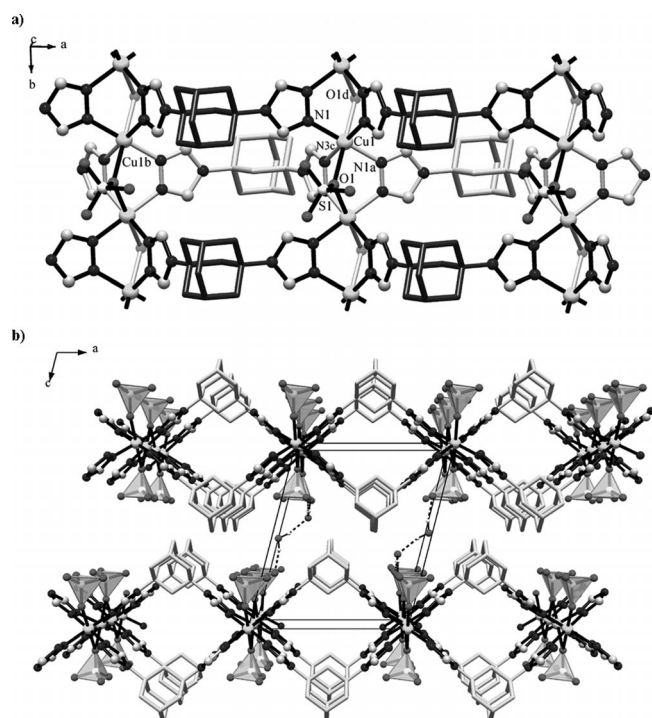


Figure 1. Formation of 2D layers in the crystal structure of **1**. (a) Cooperative coordination of Cu atoms and $\text{tr}/\text{SO}_4^{2-}$ bridges leads to $[\text{CuSO}_4(\mu\text{-}N^1, N^2\text{-tr})_2]$ column motifs, which form 2D sheets through $\mu_4\text{-tr}_{2\text{ad}}$ ligands. (b) Adjacent layers are packed together through intermolecular H-bonding interactions between SO_4^{2-} anions and uncoordinated water molecules located within the interlayer space. Symmetry codes: (a) $-x + 2, -y, -z + 2$; (b) $x + 1, y, z$; (c) $-x + 1, -y, -z + 2$; (d) $x, -y - 0.5, z$.

direction, which are separated within the layer by extended hydrophilic ribbons of $[\text{CuSO}_4(\mu\text{-}N^1, N^2\text{-tr})_2]$. Similar $\text{CuSO}_4/\mu\text{-}N^1, N^2\text{-tr}$ interactions observed earlier for linear 4-phenylene-4,4'-bi(1,2,4-triazole) afforded a 3D framework with wide rectangular channels.^[16] In **1**, the neighboring layers are held together by multiple noncovalent interactions between the aliphatic parts, and the hydrophilic regions along the $\text{Cu}(\mu\text{-SO}_4)$ columns are stabilized by intermolecular hydrogen bonding with uncoordinated water molecules (Figure 1b). Thus, the molecules of water are settled inside the interlayer channels of a slightly larger size (a diagonal cross-section of $2 \times 4 \text{ \AA}$).

The crystal structure of **2** consists of trinuclear linear units $[\text{Cu}_3(\mu\text{-}N^1, N^2\text{-tr})_6]$ arranged in 2D layers by two kinds of tri- and tetradentate double-bridged $\text{tr}_{2\text{ad}}$ ligands in a 1:1 ratio (Figures 2 and 3). The centrosymmetric trinuclear SBUs are arranged parallel to the ac plane with average spacing of 11.19 and 14.96 \AA along the crystallographic a and c axes, respectively. In the $[\text{Cu}_3(\mu\text{-}N^1, N^2\text{-tr})_6]$ unit, the central Cu1 atom is surrounded by six N atoms of tr rings, whereas the distorted octahedral environment of the terminal Cu2 atom is completed by four N atoms of tr , a *cis*-disposed monocoordinated sulfate anion (Cu2-O5 2.887 \AA) and a water molecule (Cu2-O1 1.958 \AA). Both H_2O molecules and SO_4^{2-} anions are involved in intramolecular H bonding ($\text{O1}\cdots\text{O4}$ 2.675 \AA , $\angle\text{O1-H1W}\cdots\text{O4}$ 165.6 $^\circ$), which

Table 2. Selected bond lengths [\AA] and angles [$^\circ$] for **1–3**.

$[\text{Cu}(\text{tr}_{2\text{ad}})(\text{SO}_4)] \cdot 3\text{H}_2\text{O}$ (**1**) symmetry codes: (a) $-x + 2, -y, -z + 2$; (b) $x + 1, y, z$; (c) $-x + 1, -y, -z + 2$.

Cu1–N1a	$2 \times 2.008(2)$	N1a–Cu1–O1a	94.89(11)
Cu1–N3b	$2 \times 2.012(3)$	N1–Cu1–O1a	85.11(11)
Cu1–O1	$2 \times 2.406(2)$	N3b–Cu1–O1a	85.80(11)
		N3c–Cu1–O1a	94.20(11)
N1a–Cu1–N1	180.0	N1a–Cu1–O1	85.11(11)
N1a–Cu1–N3b	91.71(10)	N1–Cu1–O1	94.89(11)
N1–Cu1–N3b	88.29(10)	N3b–Cu1–O1	94.20(11)
N1–Cu1–N3c	91.71(10)	N3c–Cu1–O1	85.80(11)

$[\text{Cu}_3(\text{tr}_{2\text{ad}})_4(\text{H}_2\text{O})_2(\text{SO}_4)_2] \text{SO}_4 \cdot 28\text{H}_2\text{O}$ (**2**), symmetry codes: (b) $-x, -y, -z$; (c) $-x + 1, -y, -z$; (d) $x - 1, y, z$; (e) $-x, -y, -z + 1$.

Cu1–N7	$2 \times 2.0239(13)$	N7b–Cu1–N11d	90.03(5)
Cu1–N1	$2 \times 2.0340(12)$	N1–Cu1–N11c	86.76(5)
Cu1–N11c	$2 \times 2.3651(13)$	O1–Cu2–N10c	89.29(5)
Cu2–O1	1.9581(12)	O1–Cu2–N5e	86.49(5)
Cu2–N10c	1.9955(13)	N10c–Cu2–N5e	175.78(5)
Cu2–N5e	2.0062(13)	O1–Cu2–N2	161.18(5)
Cu2–N2	2.0321(14)	N10c–Cu2–N2	95.24(5)
Cu2–N8b	2.2230(13)	N5e–Cu2–N2	88.85(5)
		O1–Cu2–N8b	109.78(5)
N7–Cu1–N7b	180.0	N10c–Cu2–N8b	88.87(5)
N7–Cu1–N1	88.19(5)	N5e–Cu2–N8b	92.29(5)
N7b–Cu1–N1	91.81(5)	N2–Cu2–N8b	88.61(5)

$[\text{Cu}_3(\text{tr}_{2\text{ad}})_4(\text{H}_2\text{O})_4](\text{SiF}_6)_3 \cdot 16\text{H}_2\text{O}$ (**3**), symmetry codes: (a) $-x + 1, -y + 2, -z$; (b) $-x + 2, -y + 2, -z$; (c) $x - 1, y, z$; (d) $x, y, z - 1$; (e) $-x + 1, -y + 2, -z + 1$.

Cu1–N1	$2 \times 2.002(2)$	N5b–Cu1–N11d	90.30(9)
Cu1–N5b	$2 \times 2.035(2)$	O1–Cu2–N7	88.17(10)
Cu1–N11d	$2 \times 2.413(2)$	O1–Cu2–N10e	179.11(9)
Cu2–O1	1.987(2)	N7–Cu2–N10e	91.04(10)
Cu2–N10e	1.999(2)	N7–Cu2–N2	169.20(10)
Cu2–N2	2.021(2)	N10e–Cu2–N2	92.74(10)
Cu2–N4c	2.269(2)	O1–Cu2–N4c	88.56(9)
		N7–Cu2–N4c	98.51(10)
N1–Cu1–N1a	180.0	N10d–Cu2–N4c	91.17(9)
N1–Cu1–N5b	88.69(9)	N2–Cu2–N4c	91.53(9)
N1–Cu1–N11d	90.24(9)		

is presumably the crucial factor that prevents additional $\text{tr}_{2\text{ad}}$ coordination. The other uncoordinated water molecules and sulfate anions are housed within the interlayer space and form a hydrogen-bonded network.

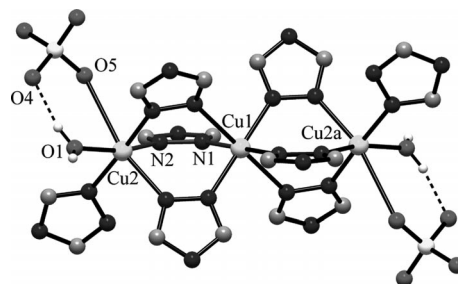


Figure 2. A linear trinuclear cluster $[\text{Cu}_3(\mu\text{-}N^1, N^2\text{-tr})_6(\text{SO}_4)_2(\text{H}_2\text{O})_2]$ motif in the structure of **2**. Symmetry code: (a) $1 - x, -y, 1 - z$.

The $\text{CuSO}_4/\text{tr}_{2\text{ad}}/\text{H}_2\text{O}$ system is remarkably sensitive to reaction conditions (especially to the pH value) and, thus, leads to various products or their mixtures (see Experimental Section). This causes synthetic difficulties in controlling

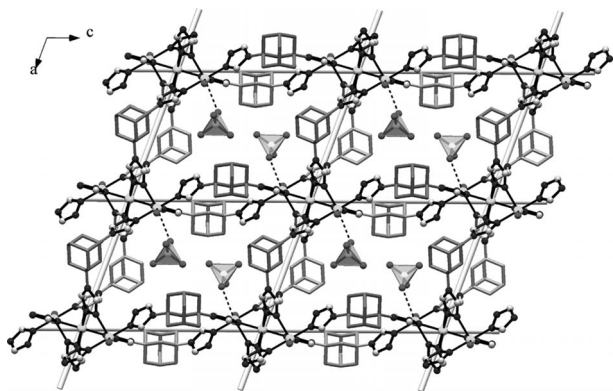


Figure 3. Formation of a square-grid network in the crystal structure of **2**, in which the linear clusters $[\text{Cu}_3(\mu\text{-}N^i, N^j\text{-tr})_6]$ act as nodes.

the phase purity of the samples, which is especially important for correct interpretation of the magnetic data. We found that crystallization experiments with aqueous CuSiF_6 and tr_2ad under normal hydrothermal conditions afforded

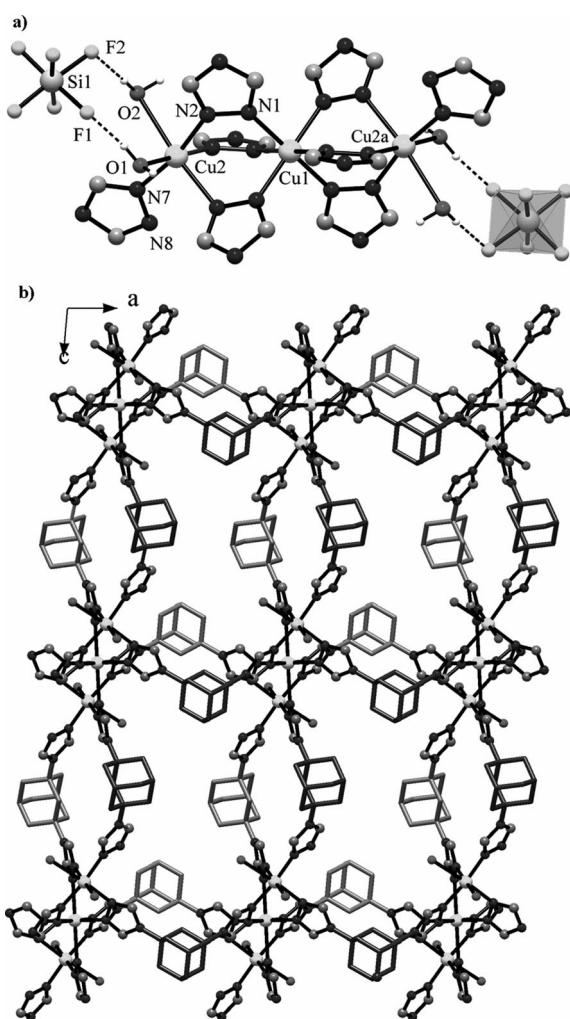


Figure 4. Crystal structure of **3**. (a) Structure of the $[\text{Cu}_3(\mu\text{-}N^i, N^j\text{-tr})_6(\text{H}_2\text{O})_4](\text{SiF}_6)_2$ fragment. (b) Integration of the cluster motifs into the 2D network.

pure blue prismatic crystals with composition $[\text{Cu}_3(\text{tr}_2\text{ad})_4(\text{H}_2\text{O})_4](\text{SiF}_6)_3 \cdot 16\text{H}_2\text{O}$ (**3**). The crystal structure of **3** consists of trinuclear $[\text{Cu}_3(\mu\text{-}N^i, N^j\text{-tr})_6]$ clusters, which are organized into square-grid networks by μ_3 - and μ_4 -double-bridged tr_2ad ligands (Figure 4). The interlinked SBU's are located within the layer at distances of 11.25 and 15.63 Å. Thus, the structural features and the $[\text{Cu}_3(\mu\text{-}N^i, N^j\text{-tr})_6]$ cluster geometry are similar to those of **2**: six tr moieties linearly bridge three copper centers with a $\text{Cu1}\cdots\text{Cu2}$ distance of 3.756 Å. However, because of the weak nucleophilic properties of SiF_6^{2-} , the distorted Cu (peripheral) octahedra are filled by four N atoms of tr and two aqua ligands. The uncoordinated SiF_6^{2-} anions and water molecules form a set of hydrogen-bonding interactions ($\text{O1}\cdots\text{F1}$ 2.595, $\text{O2}\cdots\text{F2}$ 2.883 Å). The porosity of the framework was estimated by using the PLATON program:^[22] the solvent-accessible volume, after removing the uncoordinated water molecules and counteranions, is calculated to be 765.9 Å³ (or 37.0% of the unit cell).

To evaluate the thermal stability of **3**, the sample was examined by high-temperature powder X-ray diffraction (PXRD, Figure 5). The data show that the coordination framework remains stable up to 190 °C, whereas further temperature increase from 190 to 330 °C leads to an irreversible decomposition process with loss of crystallinity.

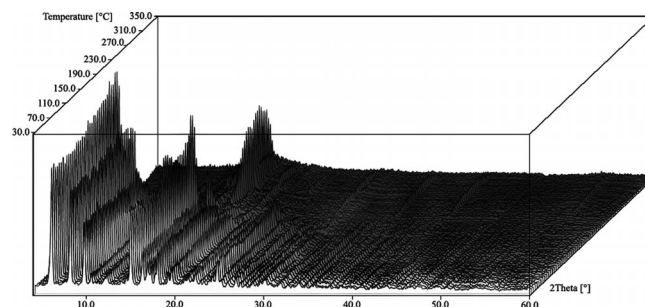


Figure 5. Temperature-dependent PXRD pattern ($2\theta = 0\text{--}60^\circ$) for $[\text{Cu}_3(\text{tr}_2\text{ad})_4(\text{H}_2\text{O})_4](\text{SiF}_6)_3 \cdot 16\text{H}_2\text{O}$ (**3**).

Magnetic Susceptibility

The temperature dependence of the effective magnetic moment indicates a weak antiferromagnetic interaction in trimer **3** (Figure 6). The room-temperature magnetic moment of ca. $3.15 \mu_B$ is consistent with three noninteracting $S = 1/2$ ions with a g_{average} value of 2.1. However, when the temperature is lowered, the magnetic moment decreases slowly to $3 \mu_B$ at ca. 40 K and then more quickly to $1.86 \mu_B$ at 1.8 K. The latter value indicates that only the $S = 1/2$ state of the trinuclear system is populated at 1.8 K. The trimer is centrosymmetric, and the Heisenberg–Dirac–Van Vleck (HDVV) Hamiltonian should take the form in Equation (1), in which the central atom has number 2.

$$\hat{H} = J_1(\hat{S}_1\hat{S}_2 + \hat{S}_2\hat{S}_3) + J_2\hat{S}_1\hat{S}_3 \quad (1)$$

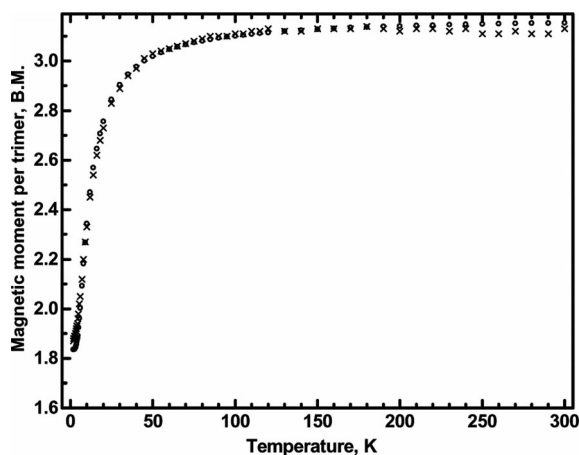


Figure 6. Temperature dependence of μ_{eff} for $[\text{Cu}_3(\text{tr}_2\text{ad})_4(\text{H}_2\text{O})_4]-(\text{SiF}_6)_3 \cdot 16\text{H}_2\text{O}$ (**3**). Circles: experimental; dots: calculated from Equation (4) with $J_1 = 9.8 \text{ cm}^{-1}$, $J_2 = 0 \text{ cm}^{-1}$ and $g = 2.115$.

The J_2 value is likely to be very small compared to J_1 .

The exchange interactions in a system of three $S = 1/2$ ions give rise to one quartet state ($S = 3/2$) and two doublet states ($S = 1/2$). These states can be labeled as $|S_T, S'\rangle$ by using their “intermediate spin” $S' = S_1 + S_3$ and the “total spin”, $S_T = S_1 + S_2 + S_3 = S' + S_2$. The symbols Q, D1 and D2 will be used for the quartet state $|3/2, 1\rangle$ and the doublet states $|1/2, 1\rangle$ and $|1/2, 0\rangle$, respectively.

In a simple system with only two different exchange integrals, one can apply Kambe’s method to calculate the energies of the (S_T, S') levels of a trimer^[23] [Equation (2)].

$$E(S_T, S') = (J_1/2)S_T(S_T + 1) + (J_2/2 - J_1/2)S'(S' + 1) - (3/8)J_1 - (3/4)J_2 \quad (2)$$

These energies result in Equation (3) for the trimer magnetic susceptibility.

$$\chi = \frac{Ng^2\mu_B^2}{3kT} \frac{15e^{-(J_1/2+J_2/4)/kT} + 1.5e^{-(J_1+J_2/4)/kT} + 1.5e^{-3J_2/4kT}}{4e^{-(J_1/2+J_2/4)/kT} + 2e^{-(J_1+J_2/4)/kT} + 2e^{-3J_2/4kT}} \quad (3)$$

Equation (3) is equivalent to that derived in ref.^[24] (which uses the opposite sign convention for J). Fitting of the magnetic data with J_2 fixed to 0 resulted in $J_1 = 9.8 \text{ cm}^{-1}$ and $g = 2.115$, and the ground state is the doublet, D1, with $S_T = 1/2$, $S' = 1$. Neglecting J_2 is justified by the results of the DFT calculations (see below).

EPR Spectra

The high-field EPR spectra are consistent with the picture emerging from the magnetic data. The spectrum of a quartet spin state ($S = 3/2$) is visible at all temperatures, except the lowest we can reach (ca. 3 K). Spectra of $S = 1/2$ states are also seen (Figures 7 and 8), which, however, become weaker when the temperature is raised so that only the $S = 3/2$ state is seen at room temperature.

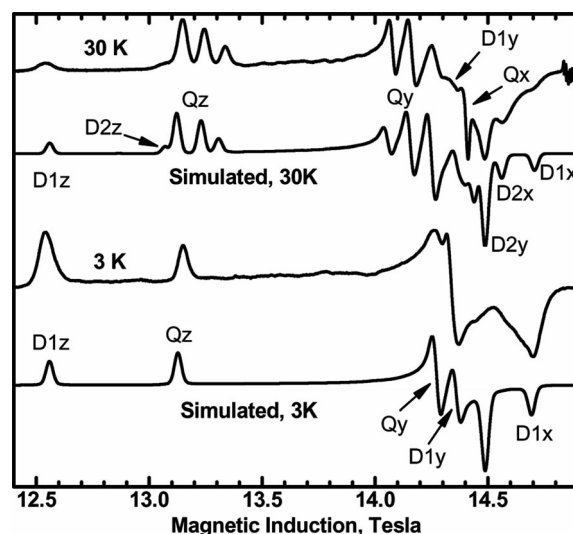


Figure 7. EPR spectra of **3** recorded at temperatures indicated with the microwave frequency $\nu = 416.00 \text{ GHz}$. Resonances are labeled Q for quartet and D1, D2 for the doublet states. D1 is the ground state. Indices x, y, and z indicate the orientations of the respective g tensors vs. the magnetic field. Note that one Q_z and one Q_y component persist at 3 K, because the Zeeman interaction lowers the energy of the $M_S = -3/2$ level of the quartet state almost to that of $M_S = -1/2$ level of D1 in this magnetic field range (see Figure 9). The parameters in Table 4 were used in simulations. The pattern seen at the high-field end of the 30 K spectrum is caused by Mn^{II} in the gelatin cap used as a sample container.

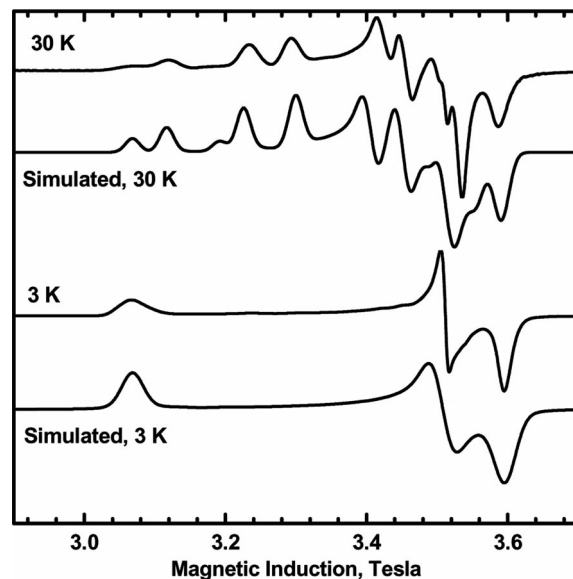


Figure 8. EPR spectra of **3** recorded at temperatures indicated with the microwave frequency $\nu = 101.6 \text{ GHz}$. At 3 K a pure spectrum of the D1 doublet is observed, because in this magnetic field range D1 is a well-isolated ground state (see Figure 9).

The interpretation of the EPR spectra proved to be very challenging. The quartet state spectrum would normally be simulated using the spin Hamiltonian [Equation (4)]

$$\hat{H} = \mu_B B \cdot g \cdot \hat{S} + D\{\hat{S}_z^2 - S(S+1)/3\} + E(\hat{S}_x^2 - \hat{S}_y^2) \quad (4)$$

with $S = 3/2$. As a matter of fact, the spectrum shown in Figure 7 can be seemingly satisfactorily simulated as a sum

of a quartet with $g_x = 2.062$, $g_y = 2.097$, $g_z = 2.244$, $D = -0.0503 \text{ cm}^{-1}$, $E = -0.0159 \text{ cm}^{-1}$, and of two doublet spectra with $\{g\}_{D1}$ and $\{g\}_{D2}$ components, respectively, given in Table 3. However, the splittings within the y and z groups of the experimental resonances of the $S = 3/2$ state (Figures 7 and 8) are frequency-dependent, which cannot be reproduced by Hamiltonian (5). This behavior indicates that the quartet state is not a “pure” state. The eight $|S, M_S\rangle$ wave functions of the trinuclear unit can be expressed as combinations of the α and β functions of separate copper ions, representing $m_s = 1/2$ and $-1/2$, respectively [see Formula (1) in the Supporting Information].

Table 3. EPR parameters for 3.

g values ^[a]	g_x	g_y	g_z
Central Cu ^{II} , $\{g\}_2$ ^[b]	2.041	2.054	2.274
Terminal Cu ^{II} , $\{g\}_1$ ^[c]	2.074	2.057	2.302
Doublet D1, $\{g\}_{D1}$ exp. ^[b]	2.022	2.073	2.370
Calcd. ^[c]	2.019	2.070	2.367
Quartet, $\{g\}_Q$, exp. ^[d]	2.051	2.097	2.244
Calcd. ^[c]	2.058	2.103	2.250
Cu–Cu interactions	D [cm ⁻¹]	E [cm ⁻¹]	J [cm ⁻¹]
Cu1–Cu2 and Cu2–Cu3	-0.175	-0.040	10.5
Cu1–Cu3 ^[e]	-0.013	0	0

[a] Each set of g values refers to its own system of axes, see Supporting Information. [b] Obtained directly from the spectra. [c] Obtained from fitting of the experimental g values in doublet D1 and in the quartet, see text. [d] Obtained from the spectrum at the position of the central quartet resonance line at the respective orientation. [e] D calculated from the point-dipole model, Equation (8).

These spin functions are, in the absence of magnetic field and zero-field splitting (zfs), the eigenfunctions of the HDVV Hamiltonian (1) as well as of the total spin-square operator $\hat{S}^2 = (\hat{S}_1 + \hat{S}_2 + \hat{S}_3)^2$.

However, in a magnetic field they mix, and the degree of mixing depends on the separation between the spin multiplets. Although the spin Hamiltonian (4) would be correct for a trimeric complex with strong exchange interactions, it is inadequate in the present case. A correct procedure is to apply a spin Hamiltonian that contains the spin operators of three copper ions [Equation (5)].

$$\hat{H} = \mu_B B \{g\}_1 \hat{S}_1 + \mu_B B \{g\}_2 \hat{S}_2 + \mu_B B \{g\}_3 \hat{S}_3 + \hat{S}_1 \{D\}_{12} \hat{S}_2 + \hat{S}_2 \{D\}_{12} \hat{S}_3 + \hat{S}_1 \{D\}_{13} \hat{S}_3 \quad (5)$$

According to the molecular symmetry, the tensors $\{g\}_1$ and $\{g\}_3$ must be equal. The zero-field splitting tensors $\{D\}_{12}$ and $\{D\}_{23}$ must be equal, and they include the isotropic exchange interaction represented by J_1 plus the anisotropic exchange and the dipole–dipole interactions. The Dzialoshinskii–Moriya interaction was not considered, because the complex has an inversion center.^[25]

The interaction $\{D\}_{13}$ may be negligible, apart from a small dipole–dipole contribution, which is eight times smaller than the dipolar contribution to $\{D\}_{12}$ because of the doubled Cu–Cu distance. That contribution was taken into account in simulations.

The application of the spin Hamiltonian (5) is difficult because of many unknown quantities starting from the g

tensors. DFT calculations (below) indicate that the unpaired electrons of all three copper ions are in the respective $d_{x^2-y^2}$ orbitals. One large g component (g_z) and two smaller ones that are close to each other (g_x and g_y) are typically expected in such a situation. There are not many published EPR parameters of monomeric copper–triazole complexes. Copper(II) doped into an iron(II)–bitriazole complex and surrounded by four triazole nitrogen atoms in its equatorial plane exhibited $g_{x,y} = 2.06$, $g_z = 2.28$,^[26] and the central copper ion in our trimer may be expected to have g values of similar magnitude. The g components of the terminal copper atoms may be somewhat larger than those of the central copper atom, as the former ones have an equatorial N₃O coordination. The ground doublet state, the spectrum of which emerges at low temperatures, exhibits $g_x = 2.022$, $g_y = 2.073$, $g_z = 2.370$, which do not appear correct for Cu^{II} coordinated by nitrogen atoms. One has to bear in mind that we do not observe g of a single copper ion here, but rather a combination of differently oriented g tensors of all three copper ions. By working with the operator $g_{1z} \hat{S}_{z1} + g_{2z} \hat{S}_{z2} + g_{3z} \hat{S}_{z3}$ upon the wave functions of the coupled system (see Supporting Information) one can easily prove Equation (6).

$$\begin{aligned} \{g\}_Q &= (\{g\}_1 + \{g\}_2 + \{g\}_3)/3 = (2\{g\}_1 + \{g\}_2)/3 \\ \{g\}_{D1} &= (4\{g\}_1 - \{g\}_2)/3 \\ \{g\}_{D2} &= \{g\}_2 \end{aligned} \quad (6)$$

Q, D1 and D2 represent the quartet, the ground doublet $S_T = 1/2$, $S' = 1$ and the intermediate doublet state, $S_T = 1/2$, $S' = 0$, respectively (see also Table 3.4 in ref.^[27]). The direction of the g_z component in a $d_{x^2-y^2}$ copper ion is expected to be perpendicular to the plane of the equatorial ligands. In our system this is likely to be obeyed, particularly for the central copper atom. However, the equality of the g_x and g_y components is not guaranteed for the central copper atom, and less yet for the terminal copper atoms. The z axes of the terminal copper atoms as defined here are inclined by 58° with respect to the z axis of the central copper atom. The mechanism for creating unusual g values in the ground doublet state relies on that misalignment. To illustrate this effect let us assume for simplicity that the z axis of the central atom is parallel to the x axes of the terminal atoms, that all y axes are parallel, and that $g_x = g_y = 2.060$, $g_z = 2.280$ for both terminal and central atoms. This would result in three different g values in the ground doublet, one of which is smaller than 2 [$g'_x = (4g_x - g_z)/3 = 1.99$, $g'_y = 2.06$, $g'_z = (4g_z - g_x)/3 = 2.35$] and in the quartet state $g'_x = 2.133$, $g'_y = 2.06$, $g'_z = 2.206$.

Interestingly, Aznar et al. observed g parameters very similar to those of our lowest-temperature spectra ($g_1 = 2.00$, $g_2 = 2.07$ and $g_3 = 2.39$) in the Q-Band EPR spectrum of a linear trinuclear copper–guanazole complex at 4.2 K.^[24] These values are obviously caused by the effect described above and that the complex is likely to produce high-field EPR spectra similar to ours.

The real situation is more complicated because of the non-90° arrangement of the g tensors. To handle this, sys-

tems of coordinates have been tentatively set up on the central and terminal copper ions, with the z axes perpendicular to the plane of the equatorial ligands. The g values of the central atom have been determined thanks to the identification of the signals owing to the intermediate doublet state D2 in the EPR spectra (Figure 7). They are $g_{2x} = 2.041$, $g_{2y} = 2.055$, $g_{2z} = 2.274$. To determine the $\{g\}_1$ components of the terminal atoms, a least-squares procedure searched for the g_{1x} , g_{1y} , and g_{1z} values that would reproduce the g values of the quartet and ground doublet states observed in experimental spectra ($\{g\}_Q$ and $\{g\}_{D1}$), respectively. To accomplish this, the $\{g\}_1$ tensor was transformed into the central copper ion coordinates, and Equation (8) was applied to calculate $\{g\}_Q$ and $\{g\}_{D1}$, which were subsequently diagonalized. This appears to have produced sensible results, although the $\{g\}_Q$ and $\{g\}_{D1}$ components could not be perfectly reproduced even if rotation of the $\{g\}_1$ axes was allowed. The differences between the calculated and real g values were smaller than 0.01, which is, however, sufficient to cause considerable shifts in the high-frequency spectra; $g_x = 2.070$, $g_y = 2.061$, and $g_z = 2.302$ were found for the terminal atoms in this way. Next, the g values, as well as the systems of coordinates for the central and terminal atoms were used in the EPR simulation program on the basis of the spin Hamiltonian (5). At this point, the orientation of the zero-field splitting tensor $\{D\}_{12}$ had to be chosen, as there is no information to extract it from our experimental data. It was assumed that $\{D\}_{12}$ has one main axis parallel to the Cu–Cu vector. Simulation with two g tensors and the zfs interaction tensor, each of which has its own system of axes was not trivial and was time-consuming. Methods described in the literature^[28] were used.

Calculations were performed using the axes of the g tensor of the central copper atom ($\{g\}_2$) as a base. The program used as input parameters the J values as well as the D and E parameters for interactions Cu1–Cu2 and Cu1–Cu3. The respective $\{D\}$ tensor elements were calculated from $D_{xx} = J - (1/3)D + E$, $D_{yy} = J - (1/3)D - E$, and $D_{zz} = J + (2/3)D$. Tensors $\{D\}_{12}$, $\{D\}_{13}$ and $\{g\}_1$ were rotated to the axes of $\{g\}_2$ and the 8×8 (complex) matrix of Hamiltonian (5) was formed and diagonalized.^[29]

Upon finding a resonance field by an iterative procedure, the eigenvectors ψ_i and ψ_j of the levels involved in a transition were evaluated, and the relative transition probability P was calculated from terms of Equation (7)

$$P = |\langle \psi_i | U \{g\}_1 \hat{S}_1 + U \{g\}_2 \hat{S}_2 + U \{g\}_3 \hat{S}_3 | \psi_j \rangle|^2 \quad (7)$$

where U represents the unit-length vector perpendicular to the steady magnetic field B . Twelve orientations of U were used, and the resulting P values were averaged. The intensity of a transition was taken as a product of the probability P and the population difference between the levels ψ_i and ψ_j , which was obtained from the Boltzmann distribution. The above procedure was repeated thousands of times for various orientations of the steady magnetic field B to generate a powder EPR spectrum. Spectra simulated in this way are shown in Figures 7 and 8. The main source of discrepancy between the simulated and experimental traces are the

slightly incorrect g values. Attempts to orient the $\{D\}_{12}$ tensor parallel to the g tensor of the quartet state were relatively less successful, as the splitting in the Z and Y parts of the quartet spectrum could not be reproduced at the same time. Interestingly, J_1 of 9.8 cm^{-1} as found from the magnetic susceptibility data could not be used in the EPR simulations, because with that J_1 there is extensive mixing and “anticrossing” of the spin multiplets at magnetic fields where our 400 GHz spectra are located causing the simulated spectra to be very different from the experiment. EPR simulations indicate that J_1 must be at least 10.5 cm^{-1} , and the spectra (Figures 7 and 8) as well as the energy levels (Figure 9) were calculated using that value.

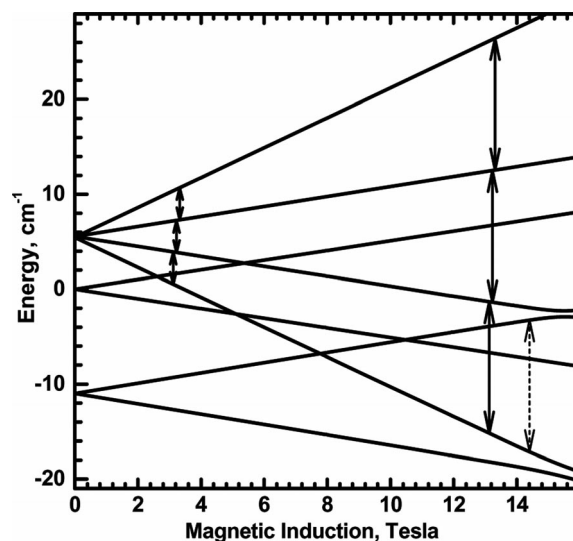


Figure 9. Energy levels of **3** in the magnetic field. The energies were calculated at the z orientation of the $\{g\}_Q$ tensor. Short and long black arrows represent the EPR transition within the quartet state at 101.6 and 416.0 GHz, respectively. At the lower microwave frequency, the quartet spectrum will be completely suppressed at low temperatures, because the transitions occur within highly excited levels. At 416 GHz, a quartet transition starting from a level that is only weakly excited is observed even at 3 K (see also Figures 7 and 8). The blue arrow shows a quartet–doublet transition, the calculated probability of which is 200 times lower than that of the interquartet transitions. “Anti-crossing” effects caused by mixing of the D1 doublet and the quartet state are seen at magnetic field above 14 T.

The best values of the D and E parameters for both interactions Cu1–Cu2 and Cu2–Cu3 were $D = -0.175 \text{ cm}^{-1}$ and $E = -0.040 \text{ cm}^{-1}$ (Table 4). The dipole–dipole contribution to D can be estimated from the point-dipole model [Equation (8)],

$$D_{\text{dipole}} = -3g^2\mu_B^2/R^3_{\text{Cu-Cu}} \quad (8)$$

which results in a contribution of -0.108 cm^{-1} to D_{12} and D_{23} and -0.0135 cm^{-1} to D_{13} . The model that takes no electron delocalization into account is likely to overestimate D .^[30]

It appears thus that anisotropic exchange must contribute to D_{12} . The theory of that contribution is extremely complicated even in simple copper acetate dimers.^[30,31] It depends on an exchange interaction within a pair of ions in

Table 4. Crystal data for [Cu(tr₂ad)(SO₄)]·3H₂O (1), [Cu₃(tr₂ad)₄(H₂O)₂(SO₄)₂]SO₄·28H₂O (2), [Cu₃(tr₂ad)₄(H₂O)₄](SiF₆)₃·16H₂O (3).

Compound	1	2	3
Empirical formula	C ₁₄ H ₂₄ CuN ₆ O ₇ S	C ₅₆ H ₁₃₂ Cu ₃ N ₂ O ₄₂ S ₃₄	C ₅₆ H ₁₁₂ Cu ₃ F ₁₈ N ₂₄ O ₂₀ Si ₃
<i>T</i> [K]	213	173	173
<i>M</i>	483.99	2100.66	2058.59
Crystal system	monoclinic	triclinic	triclinic
Space group, <i>Z</i>	<i>P</i> 2 ₁ / <i>m</i> , 2	<i>P</i> $\bar{1}$, 1	<i>P</i> $\bar{1}$, 1
<i>a</i> [Å]	10.7779(11)	11.1872(3)	11.2456(3)
<i>b</i> [Å]	7.0648(5)	14.6275(4)	12.6499(4)
<i>c</i> [Å]	12.9275(12)	14.9571(4)	15.6257(5)
α [°]	90	103.113(2)	107.2050(10)
β [°]	104.377(10)	107.710(2)	91.0660(10)
γ [°]	90	96.277(2)	102.065(2)
<i>V</i> [Å ³]	953.52(15)	2228.44(10)	2068.76(11)
μ (Mo- <i>K</i> α) [mm ⁻¹]	1.307	0.884	0.930
<i>D</i> _{calcd.} [g cm ⁻³]	1.686	1.565	1.652
θ _{max} [°]	27.48	29.57	26.15
Measured/unique reflections	6355/1892	42291/12450	21267/8074
<i>R</i> _{int}	0.0526	0.0307	0.0335
Parameters refined	155	610	484
<i>R</i> ₁ , <i>wR</i> ₂ [<i>I</i> > 2σ(<i>I</i>)]	0.046, 0.117	0.032, 0.082	0.046, 0.128
<i>R</i> ₁ , <i>wR</i> ₂ (all data)	0.056, 0.120	0.045, 0.084	0.062, 0.134
Goodness-of-fit on <i>F</i> ²	0.969	0.941	1.103
Max, min peak [e ⁻ Å ⁻³]	1.18, -0.49	1.19, -0.51	0.89, -0.40

which one of the ions is in its ground state and the other one is in an excited electronic state. In the present case that estimated contribution (from the difference between the experimental *D* and *D*_{dipole}) is -0.067 cm⁻¹, which is much smaller than observed in dimeric copper carboxylates.^[30–32]

Calculation of the Exchange Integral from DFT

Interaction between the Central and Terminal Copper Atoms

We used the DFT software package ORCA^[33] to estimate the exchange integrals in our trinuclear complex **3**. The X-ray structure was used, but large organic fragments were removed, as shown in Figure 10. The software first performed a self-consistent field (SCF) calculation for the high-spin *S* = 3/2 state, then “flipped” the spin on one of the terminal copper atoms to generate the “broken-symmetry” state with *M*_S = 1/2, performed another SCF calculation for that state, and finally used the two energies found above to calculate the exchange integral, corresponding to the interaction between the central copper atom and one of the terminal ones, that is *J*₁ in spin Hamiltonian (1). The ORCA calculation utilized the Ahlrichs-type basis set TZVPP^[34a] for copper ions and all coordinated atoms, whereas SVP^[34] functions were used for the remaining atoms. The B3LYP^[35] functional was employed. Ahlrichs H–Kr polarization functions and auxiliary basis sets from the TurboMole library were also used.^[34b] The ORCA input file as well as selected output are included in the Supporting Information; ORCA uses $-2J_{ij}S_iS_j$ to express the interaction between a pair of atoms “*i*” and “*j*”, whereas the convention $J_{ij}S_iS_j$ is used in this paper. The exchange integral value reported by ORCA was thus multiplied by -2 to give *J*₁ = 8.2 cm⁻¹, which correlates very well with the experimental

*J*₁ = 9.8 cm⁻¹ (see above). Figure 10 shows the corresponding spin-up (purple-green) and spin-down (red-blue) orbitals

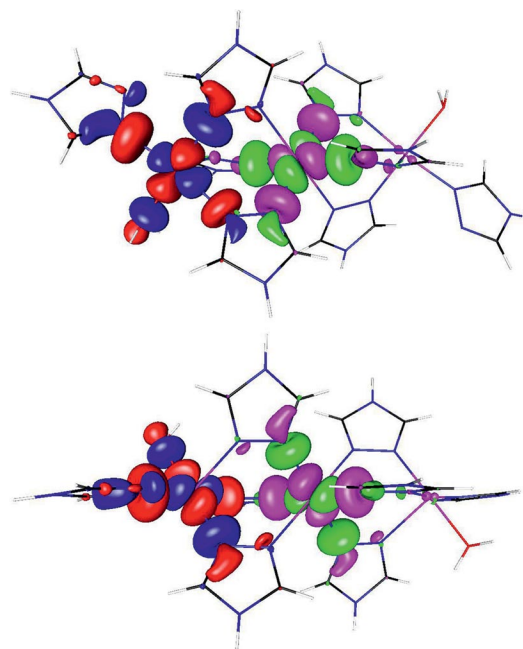


Figure 10. Two projections illustrating the “broken-symmetry” orbitals as obtained from ORCA. The positive parts of the orbitals are plotted in red and in purple. The spin-up and spin-down orbitals are strongly localized in the *d*_{x²-y² orbitals of the central and the terminal copper ion, respectively. The overlap of these so-called magnetic orbitals affects the exchange integral magnitude. It is seen that the unpaired electron density delocalizes only towards the equatorial ligands of respective copper ions. The antiferromagnetic exchange pathway is the one involving a ligand equatorial with respect to each copper ion (bottom of the upper plot). Note that the orbital based on the terminal copper atom is oriented differently to that on the central copper atom.}

als of the “broken-symmetry” solution, the overlap of which determines the exchange integral magnitude. In the present case, the overlap integral is 0.035.

The J_1 value of 8.2 cm^{-1} calculated above represents the sum of contributions from all exchange pathways in the system. We will label the pathways involving the triazole fragments containing the coordinated atoms (N1, N2), (N4, N5), and (N10, N11) (see Figure S4), with letters A, B, and C, respectively, so that J_1 should be equal in an ideal case to $J_A + J_B + J_C$. The triazole in pathway A supplies an equatorial N1 ligand to the central copper atom and an equatorial N2 ligand to the terminal copper atom. In B, the N5 atom is an equatorial ligand of the central copper atom (2.035 \AA), and N4 is an axial ligand of the terminal copper atom (2.269 \AA). Finally, in C, the N10 atom is coordinated equatorially to the terminal copper atom (1.999 \AA), and N11 is an axial ligand of the central copper atom at a relatively long distance of 2.413 \AA . The latter two pathways are expected to result in ferromagnetic contributions J_B and J_C to the exchange interactions, whereas the first one should transmit an antiferromagnetic interaction J_A . We have performed additional DFT calculations for molecules in which one or both ferromagnetic exchange pathways (B and C) were destroyed. In the first calculation, the (N4, N5) triazole was removed, and NH_3 was created at the site of N5, thus removing pathway B. This change was introduced only to the Cu1–Cu2 part of the trimer where ORCA’s spin flip was to be accomplished, leaving the symmetry-related triazole between Cu2 and Cu3 in place. This resulted in the exchange integral value of 9.7 cm^{-1} from DFT, which in an ideal case would represent $J_A + J_C$. The slight increase in the antiferromagnetic interaction from 8.2 to 9.7 cm^{-1} can be interpreted to be the result of the removal of a weak ferromagnetic contribution J_B . In the second calculation, the (N10, N11) triazole was removed, and NH_3 was created on the site of N10 to destroy pathway C. DFT calculations produced 21.2 cm^{-1} , which again may be understood to be a result of the removal of a ferromagnetic pathway J_C , although the amount of the increase appears to be too large. Finally, in the third calculation both triazole bridges were replaced by NH_3 molecules. The resulting system still retained the equatorial-to-equatorial bridge A formed by the (N1, N2) triazole, and an antiferromagnetic $J_A = 10.0 \text{ cm}^{-1}$ was obtained in this case. The molecules used in these calculations are shown in Figure S9. The calculations described here give a picture that is qualitatively in agreement with expectations, but no numerical values can be assigned to the three interactions J_A , J_B , and J_C , which would add up to give J_1 . This is due to the limited accuracy of the exchange integral determination from DFT as well as, presumably, to the disturbance caused to the molecules when the triazole bridges were removed.

Interaction between the Terminal Copper Atoms

Although the ORCA spin flip on the terminal Cu1 allows the calculation of the exchange integral between Cu1 and Cu2, this cannot be applied to evaluate the exchange inte-

gral J_2 between the terminal Cu1 and Cu3. For this reason we performed calculations on a molecule with the central copper atom replaced by a zinc atom. This resulted in a J_2 value of 0.16 cm^{-1} . Neglecting this exchange interaction in the magnetic susceptibility calculations is thus justified, as was done above and in ref.^[24]

The overall exchange integral in **3** is quite small compared to those of some linear trinuclear copper complexes bridged by two triazole ligands and one different bridge such as chloride. There are two groups of such compounds, in the first two triazole molecules join the equatorial positions of two copper ions, and the exchange integrals are above 75 cm^{-1} .^[36] In the second group, there is one equatorial-to-equatorial and one equatorial-to-axial triazole, and the exchange integrals are about 35 cm^{-1} .^[14,24,37] In our system, two ferromagnetic pathways reduce the overall antiferromagnetic interaction even more, which results in an (experimental) J_1 value of 9.8 cm^{-1} .

For comparison with our system, we performed DFT calculations on the linear copper–guanazole trimer $\{[\text{Cu}_3(\mu_2\text{-Cl})(\text{guanazole})_4(\text{H}_2\text{O})_4]^{4+}$, Figure 11} using the X-ray structure from ref.^[24] $J_1 = 102 \text{ cm}^{-1}$ was obtained, whereas the experimental value was 90 cm^{-1} .^[24] The overlap integral between the magnetic orbitals was 0.091. When the axial-to-axial chlorido bridge was removed, the calculation produced $J_1 = 100 \text{ cm}^{-1}$, which implies that the exchange pathway through the Cl^- anion is weakly antiferromagnetic, whereas the two equatorial-to-equatorial triazole bridges transmit the bulk of the antiferromagnetic interaction.

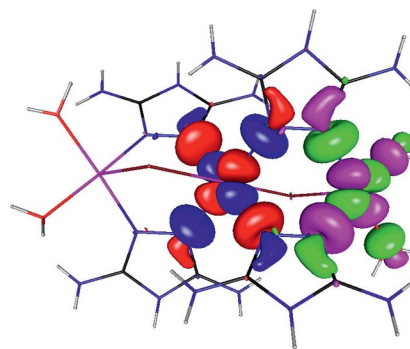


Figure 11. Illustration of the exchange pathways in $[\text{Cu}_3(\mu_2\text{-Cl})(\text{guanazole})_4(\text{H}_2\text{O})_4]^{4+}$ (the structure for DFT calculations was taken from ref.^[24]). Note that the orbitals of the central and terminal copper atoms are oriented differently.

Conclusions

This study demonstrates the potential utility of a geometrically rigid bis(triazole) ligand (tr₂ad) with an adamantane-linker platform in the structural design of Cu^{II} –MOFs. The integrated discrete linear $[\text{Cu}_3(\mu_2\text{-tr})_6]$ clusters and $[\text{Cu}(\mu_2\text{-tr})_2(\mu_2\text{-SO}_4)]$ chains, which were found to be the two principal motifs in the 2D coordination nets, are realized in the $\text{CuSO}_4/\text{tr}_2\text{ad}/\text{H}_2\text{O}$ and $\text{CuSiF}_6/\text{tr}_2\text{ad}/\text{H}_2\text{O}$ systems. Even a

slight difference in nucleophilicity of anions (SO₄²⁻ vs. SiF₆²⁻) dictates the formation of the preferred [Cu₃-(μ₂-tr)₆] motif. The CuSO₄/tr₂ad/H₂O system is very sensitive to reaction conditions and afforded diverse structures. These structural features are an essential tool for the tuning of the magnetic properties of the frameworks and may be very valuable for further studies of polyfunctional (tri- and tetra-)adamantane derivatives. The exchange integral in **3**, found from the magnetic data, could be reasonably reproduced by a broken-symmetry DFT calculation. Spin Hamiltonian parameters for **3**, which were found from high-field EPR spectra, indicate a small contribution from the anisotropic exchange interactions to the zero-field splitting.

Experimental Section

General: All chemicals were of reagent grade and were used as received without further purification. The triazole ligand was prepared by an acid-catalyzed condensation of 1,3-diaminoadamantane and *N,N*-dimethylformamide azine according to a published procedure.^[17b] X-ray powder diffraction analysis (XRPD) was performed with a STOE STADIP powder diffraction system equipped with an image plate detector with monochromated Mo-*K*_α radiation ($\lambda = 0.71073 \text{ \AA}$) in the temperature range 20–600 °C. Elemental analyses (C, H, and N) were performed with a Perkin–Elmer 2400 analyzer. IR spectra were recorded as KBr pellets with a UR-10 spectrometer (4000–400 cm⁻¹).

Synthesis of Complexes 1–3: Complexes [Cu(tr₂ad)(SO₄)]·3H₂O (**1**), [Cu₃(tr₂ad)₄(H₂O)₂(SO₄)₂]SO₄·28H₂O (**2**), and [Cu₃(tr₂ad)₄(H₂O)₄](SiF₆)₃·16H₂O (**3**) were prepared from CuSO₄·5H₂O or CuSiF₆·6H₂O and tr₂ad by employing the standard hydrothermal conditions as follows.

1: CuSO₄·5H₂O (9.0 mg, 0.036 mmol), tr₂ad (11.2 mg 0.041 mmol), H₂WO₄·2H₂O (10.0 mg, 0.035 mmol) and water (5 mL) were placed in a 20 mL Teflon-lined stainless steel autoclave, which was heated up to 180 °C and kept at that temperature for 40 h, and then cooled down to room temp. during the next 70 h. Large blue needles of **1** were separated from the oxide phase by a flotation method in a CHBr₃/CHCl₃ solution, then washed and dried. Yield: 6.1 mg, 35%. C₁₄H₂₄CuN₆O₇S (483.99): calcd. C 34.74, H 5.00, N 17.36; found C 34.68, H 5.12, N 17.29. IR (KBr): $\tilde{\nu} = 3368$ (s), 3154 (s), 3128 (s), 3020 (m), 2924 (s), 2864 (m), 1650 (m), 1552 (s), 1448 (w), 1388 (s), 1348 (s), 1316 (m), 1220 (s), 1152 (s), 1124 (s), 1092 (s), 1028 (s), 954 (s), 862 (m), 790 (w), 736 (w), 684 (w), 642 (s), 612 (s), 464 (w) cm⁻¹.

2: A mixture of CuSO₄·5H₂O (18.5 mg, 0.074 mmol), tr₂ad (10.0 mg, 0.037 mmol), and water (8 mL) in a 15 mL sealed Pyrex tube was heated at 180 °C for 40 h and then cooled to room temp. over 70 h, which resulted in an inseparable mixture of blue crystals with similar compositions but different structural dimensionalities: [Cu₃(tr₂ad)₄(SO₄)(H₂O)₃](SO₄)₂·34H₂O^[17b] (**3D**) and complex **2** (**2D**). The products were filtered, washed with water, and dried at room temp. Yield: 12.6 mg. C₅₆H₁₃₂Cu₃N₂₄O₄₂S₃ (2100.61): calcd. C 32.02, H 6.33, N 16.00; found C 31.50, H 6.52, N 15.55.

3: Complex **3** was prepared as large blue prisms in 70% yield (13.4 mg) according to similar reaction conditions and starting from CuSiF₆·6H₂O (23.3 mg, 0.074 mmol), tr₂ad (10.0 mg, 0.037 mmol) and water (8 mL). C₅₆H₁₁₂Cu₃F₁₈N₂₄O₂₀Si₃ (2058.51): calcd. C 32.67, H 5.48, N 16.33; found C 32.72, H 5.60, N 16.38. IR (KBr): $\tilde{\nu} = 3478$ (s), 3270 (s), 3124 (s), 3100 (s), 2940

(m), 2868 (w), 1658 (m), 1538 (s), 1460 (w), 1370 (m), 1348 (m), 1328 (m), 1206 (s), 1100 (s), 1078 (s), 1056 (s), 1000 (w), 908 (w), 850 (m), 732 (s), 646 (s), 478 (m), 414 (w) cm⁻¹.

Crystallography: Crystallographic measurements were made with a Stoe Image Plate Diffraction System for **1** (numerical absorption correction with X-RED and X-SHAPE) and a Bruker APEXII CCD area-detector diffractometer for **2** and **3** (ϕ scans) with graphite-monochromated Mo-*K*_α radiation ($\lambda = 0.71073 \text{ \AA}$). The data were corrected for Lorentz-polarization effects and for the effects of absorption (multi-scans method). The structures were solved by direct methods and were refined in anisotropic approximation using SHELXS-97 and SHELXL-97^[38] (Table 2). All CH hydrogen atoms were added geometrically, with $U_{\text{iso}} = 1.2U_{\text{eq}}$ (parent C atom). Crystals of **1** exhibit non-merohedral twinning. The data frames were indexed and integrated as a two-domain system using the RECIPE/TWIN facilities implemented in the Stoe IPDS software.^[39] The data were scaled and merged to yield a single dataset of about 81% completeness owing to a partial overlap of the reflections that correspond to the different domains of the crystal. The SO₄²⁻ group showed unequal (75/25) “rotational” disorder of three non-coordinated O atoms, which was resolved without geometric restraint, and only the disordered atoms of the major contribution were refined anisotropically. In the structure of **2**, a noncoordinated SO₄²⁻ anion was disordered over a center of inversion (refined without geometric restraints, but with restrained thermal motion parameters for the oxygen atoms), and four solvent water molecules were equally disordered over closely separated positions. No H atoms were added to these solvent molecules; the other OH hydrogen atoms were located from the difference map and refined as fixed contributions with OH distances constrained to 0.85 Å and $U_{\text{iso}} = 1.5 U_{\text{eq}}$ (parent O atom). In the structure of **3**, one of two independent SiF₆²⁻ anions and three water molecules were badly disordered across a center of inversion. This disordered electron density was successfully modeled using the Squeeze routine as implemented in Platon.^[22] OH hydrogen atoms for the coordinated aqua ligand and one of the solvent molecules were located and included in the calculation using the above approach. CCDC-864088 (for **1**), -864089 (for **2**) and -864090 (for **3**) contain the supplementary crystallographic data for this paper. These data can be obtained free of charge from The Cambridge Crystallographic Data Centre via www.ccdc.cam.ac.uk/data_request/cif.

Magnetic Properties: Magnetic susceptibility data of powdered samples were measured with a Quantum Design MPMSXL-5 superconducting quantum interference device (SQUID) magnetometer (Faculty of Chemistry, Wrocław University) over the temperature range 1.8–300 K at the magnetic induction of 0.5 T. Corrections for the sample holders were applied. Diamagnetic corrections were determined from Pascal’s constants.^[40,41]

EPR Spectra: High-field, high-frequency EPR spectra at temperatures ranging from ca. 3 to 300 K were recorded with a home-built transmission spectrometer at the EMR facility of NHMFL.^[42] The microwaves were generated by a phase-locked Virginia Diodes source that generated a frequency of $13 \pm 1 \text{ GHz}$ and its harmonics of which the 2nd, 4th, 6th, 8th, 16th, 24th and 32nd were available, which resulted in a frequency range of ca. 26–432 GHz. No resonance cavity was used. A superconducting magnet (Oxford Instruments) capable of reaching a field of 17 T was employed. X-band (9.6 GHz) and Q-Band spectra (34 GHz) were recorded with a Bruker ElexSys 500E instrument (Chemistry, Wrocław University).

Supporting Information (see footnote on the first page of this article): Spectral characterization data, crystal structures and labeling schemes for compounds **1–3**.

Acknowledgments

The high-field EPR spectra were recorded at the NHMFL, which is funded by the National Science Foundation (NSF) through the Cooperative Agreement No. DMR-0654118, the State of Florida and the Department of Energy (DOE). We are also grateful to the Ministry of Science and Higher Education of Poland for financial support in the purchase of the Bruker ELEXSYS E 500 EPR spectrometer.

- [1] a) J. G. Haasnoot, *Coord. Chem. Rev.* **2000**, *200*, 131–185; b) M. H. Klingele, S. Brooker, *Coord. Chem. Rev.* **2003**, *241*, 119–132; c) U. Beckmann, S. Brooker, *Coord. Chem. Rev.* **2003**, *245*, 17–29; d) G. Aromí, L. A. Barrios, O. Roubeau, P. Gamez, *Coord. Chem. Rev.* **2011**, *255*, 485–546.
- [2] C. Janiak, *Dalton Trans.* **2003**, 2781–2804.
- [3] a) Y. Garcia, P. J. van Koningsbruggen, H. Kooijman, A. L. Spek, J. G. Haasnoot, O. Kahn, *Eur. J. Inorg. Chem.* **2000**, 307–314; b) C. L. Zilverentant, W. L. Driessen, J. G. Haasnoot, J. J. A. Kolnaar, J. Reedijk, *Inorg. Chim. Acta* **1998**, *282*, 257–260; c) H. A. Habib, J. Sanchiz, C. Janiak, *Dalton Trans.* **2008**, 1734–1744; d) Y. Garcia, G. Bravic, C. Gieck, D. Chasseau, W. Tremel, P. Gütllich, *Inorg. Chem.* **2005**, *44*, 9723–9730.
- [4] a) G. Vos, J. G. Haasnoot, G. C. Verschoor, J. Reedijk, *Inorg. Chim. Acta* **1985**, *102*, 187–198; b) G. Vos, A. J. de Kok, G. C. Verschoor, *Z. Naturforsch. B* **1981**, *36*, 809–813; c) J. J. A. Kolnaar, M. I. de Heer, H. Kooijman, A. L. Spek, G. Schmitt, V. Ksenofontov, P. Gütllich, J. G. Haasnoot, J. Reedijk, *Eur. J. Inorg. Chem.* **1999**, 881–886; d) D. W. Engelfriet, G. C. Verschoor, W. J. Vermin, *Acta Crystallogr., Sect. B* **1979**, *35*, 2927–2931; e) D. W. Engelfriet, G. C. Verschoor, W. den Brinker, *Acta Crystallogr., Sect. B* **1980**, *36*, 1554–1560; f) B. Ding, L. Yi, Y. Wang, P. Cheng, D.-Z. Liao, S.-P. Yan, Z.-H. Jiang, H.-B. Song, H.-G. Wang, *Dalton Trans.* **2006**, 665–675.
- [5] a) G. Vos, R. A. le Febvre, R. A. G. de Graaff, J. G. Haasnoot, J. Reedijk, *J. Am. Chem. Soc.* **1983**, *105*, 1682–1683; b) J. C. Liu, Y. Song, J. Z. Zhuang, X. Y. Huang, X. Z. You, *Polyhedron* **1999**, *18*, 1491–1494; c) L. R. Groeneveld, R. A. le Febvre, R. A. G. de Graaff, J. G. Haasnoot, G. Vos, J. Reedijk, *Inorg. Chim. Acta* **1985**, *102*, 69–82; d) B. Liu, L. Xu, G.-C. Guo, J.-S. Huang, *J. Mol. Struct.* **2006**, *825*, 79–86; e) O. G. Shakirova, A. V. Virovets, D. Yu. Naumov, Y. G. Shvedenkov, V. N. Elokhnina, L. G. Lavrenova, *Inorg. Chem. Commun.* **2002**, *5*, 690–693; f) B. Ding, L. Yi, W.-Z. Shen, P. Cheng, D.-Z. Liao, S.-P. Yan, Z.-H. Jiang, *J. Mol. Struct.* **2006**, *784*, 138–143; g) J. J. A. Kolnaar, G. van Dijk, H. Kooijman, A. L. Spek, V. G. Ksenofontov, P. Gütllich, J. G. Haasnoot, J. Reedijk, *Inorg. Chem.* **1997**, *36*, 2433–2440; h) Y. Garcia, P. Guionneau, G. Bravic, D. Chasseau, J. A. K. Howard, O. Kahn, V. Ksenofontov, S. Reiman, P. Gütllich, *Eur. J. Inorg. Chem.* **2000**, 1531–1538; i) M. Thomann, O. Kahn, J. Guilhem, F. Varret, *Inorg. Chem.* **1994**, *33*, 6029–6037; j) M. M. Dirtu, A. Rotaru, D. Gillard, J. Linares, E. Codjovi, B. Tinant, Y. Garcia, *Inorg. Chem.* **2009**, *48*, 7838–7852.
- [6] a) Y. Wang, P. Cheng, Y. Song, D.-Z. Liao, S.-P. Yan, *Chem. Eur. J.* **2007**, *13*, 8131–8138; b) J.-C. Liu, G.-C. Guo, J.-S. Huang, X.-Z. You, *Inorg. Chem.* **2003**, *42*, 235–243; c) M. Bichay, J. W. Fronabarger, R. Gilardi, R. J. Butcher, W. B. Sanborn, M. E. Sitzmann, M. D. Williams, *Tetrahedron Lett.* **2006**, *47*, 6663–6666; d) X.-Y. Wu, X.-F. Kuang, Z.-G. Zhao, S.-C. Chen, Y.-M. Xie, R.-M. Yu, C.-Z. Lu, *Inorg. Chim. Acta* **2010**, *363*, 1236–1242.
- [7] K. Drabent, Z. Ciunik, A. Ozarowski, *Inorg. Chem.* **2008**, *47*, 3358–3365.
- [8] a) Y. Garcia, P. J. van Koningsbruggen, G. Bravic, P. Guionneau, D. Chasseau, G. L. Cascarano, J. Moscovici, K. Lambert, A. Michalowicz, O. Kahn, *Inorg. Chem.* **1997**, *36*, 6357–6365; b) Y. Garcia, P. J. van Koningsbruggen, G. Bravic, D. Chasseau, O. Kahn, *Eur. J. Inorg. Chem.* **2003**, 356–362; c) Y. Garcia, J. Moscovici, A. Michalowicz, V. Ksenofontov, G. Levchenko, G. Bravic, D. Chasseau, P. Gütllich, *Chem. Eur. J.* **2002**, *8*, 4992–5000; d) M. Seredyuk, A. B. Gaspar, M. C. Munoz, M. Verdaguier, F. Villain, P. Gütllich, *Eur. J. Inorg. Chem.* **2007**, 4481–4491; e) K. Drabent, Z. Ciunik, *Chem. Commun.* **2001**, 1254–1255; f) J.-C. Liu, G.-C. Guo, J.-S. Huang, X.-Z. You, *Inorg. Chem.* **2003**, *42*, 235–243.
- [9] E. V. Lider, E. V. Peresypkina, A. I. Smolentsev, V. N. Elokhnina, T. I. Yaroshenko, A. V. Virovets, V. N. Ikorskii, L. G. Lavrenova, *Polyhedron* **2007**, *26*, 1612–1618.
- [10] J.-C. Liu, J.-Z. Zhuang, X.-Z. You, X.-Y. Huang, *Chem. Lett.* **1999**, 651–652.
- [11] O. Kahn in *Molecular Magnetism*, VCH, Weinheim, **1993**.
- [12] Y.-Q. Huang, X.-Q. Zhao, W. Shi, W.-Y. Liu, Z.-L. Chen, P. Cheng, D.-Z. Liao, S.-P. Yan, *Cryst. Growth Des.* **2008**, *8*, 3652–3660.
- [13] B. Ding, Y. Q. Huang, Y. Y. Liu, W. Shi, P. Cheng, *Inorg. Chem. Commun.* **2007**, *10*, 7–10.
- [14] J.-C. Liu, D.-G. Fu, J.-Z. Zhuang, C.-Y. Duan, X.-Z. You, *J. Chem. Soc., Dalton Trans.* **1999**, 2337–2342.
- [15] S. Ferrer, J. G. Haasnoot, J. Reedijk, E. Müller, M. B. Cingi, M. Lanfranchi, A. M. M. Lanfredi, J. Ribas, *Inorg. Chem.* **2000**, *39*, 1859–1867.
- [16] O. A. Bondar, L. V. Lukashuk, A. B. Lysenko, H. Krautscheid, E. B. Rusanov, A. N. Chernega, K. V. Domasevitch, *CrysrEngComm* **2008**, *10*, 1216–1226.
- [17] a) G. A. Senchyk, A. B. Lysenko, H. Krautscheid, J. Sieler, K. V. Domasevitch, *Acta Crystallogr., Sect. C* **2008**, *64*, m246–m249; b) G. A. Senchyk, A. B. Lysenko, E. B. Rusanov, A. N. Chernega, H. Krautscheid, K. V. Domasevitch, *Inorg. Chim. Acta* **2009**, *362*, 4439–4448; c) A. B. Lysenko, G. A. Senchyk, J. Lincke, D. Lässig, A. A. Fokin, E. D. Butova, P. R. Schreiner, H. Krautscheid, K. V. Domasevitch, *Dalton Trans.* **2010**, *39*, 4223–4231; d) G. A. Senchyk, A. B. Lysenko, D. Y. Naumov, V. P. Fedin, H. Krautscheid, K. V. Domasevitch, *Inorg. Chem. Commun.* **2010**, *13*, 1576–1579; e) G. A. Senchyk, A. B. Lysenko, H. Krautscheid, K. V. Domasevitch, *Inorg. Chem. Commun.* **2011**, *14*, 1365–1368.
- [18] Ag, Cd, Mn, Zn, Co, Cu/adamantane dicarboxylates: a) J.-C. Jin, Y.-Y. Wang, W.-H. Zhang, A. S. Lermontova, E. Kh. Lermontova, Q.-Z. Shi, *Dalton Trans.* **2009**, 10181–10191; b) J.-C. Jin, Y.-Y. Wang, P. Liu, R.-T. Liu, C. Ren, Q.-Z. Shi, *Cryst. Growth Des.* **2010**, *10*, 2029–2032; c) J. Zhang, Sh. Chen, R. A. Nieto, T. Wu, P. Feng, X. Bu, *Angew. Chem.* **2010**, *122*, 1289; *Angew. Chem. Int. Ed.* **2010**, *49*, 1267–1270; d) R. B. Nielsen, K. O. Kongshaug, H. Fjellvåg, *J. Mater. Chem.* **2008**, *18*, 1002–1007; e) D. J. Xu, L. Pan, T. J. Emge, X.-Y. Huang, J. Li, *Acta Crystallogr., Sect. C* **2006**, *62*, m150–m152. Ln, Th, U/adamantane dicarboxylates: f) F. Millange, C. Serre, J. Marrot, N. Gardant, F. Pellé, G. Férey, *J. Mater. Chem.* **2004**, *14*, 642–645; g) O. M. Nazarenko, J. A. Rusanova, H. Krautscheid, K. V. Domasevitch, *Acta Crystallogr., Sect. C* **2010**, *66*, m276–m279; h) K. M. Ok, D. O'Hare, *Dalton Trans.* **2008**, 5560–5562; i) J. A. Rusanova, E. B. Rusanov, K. V. Domasevitch, *Acta Crystallogr., Sect. C* **2010**, *66*, m207–m210.
- [19] Zn, Cd, Ni, Cu/adamantane tetracarboxylates: a) N. L. Rosi, J. Kim, M. Eddaoudi, B. Chen, M. O'Keeffe, O. M. Yaghi, *J. Am. Chem. Soc.* **2005**, *127*, 1504–1518; b) J. Kim, B. Chen, T. M. Reineke, H. Li, M. Eddaoudi, D. B. Moler, M. O'Keeffe, O. M. Yaghi, *J. Am. Chem. Soc.* **2001**, *123*, 8239–8247; c) B. Chen, M. Eddaoudi, T. M. Reineke, J. W. Kampf, M. O'Keeffe, O. M. Yaghi, *J. Am. Chem. Soc.* **2000**, *122*, 11559–11560.
- [20] J. M. Taylor, A. H. Mahmoudkhani, G. K. H. Shimizu, *Angew. Chem.* **2007**, *119*, 809; *Angew. Chem. Int. Ed.* **2007**, *46*, 795–798.
- [21] a) D. J. Hoffart, S. A. Dalrymple, G. K. H. Shimizu, *Inorg. Chem.* **2005**, *44*, 8868–8875; b) D. J. Hoffart, A. P. Côté, G. K. H. Shimizu, *Inorg. Chem.* **2003**, *42*, 8603–8605.
- [22] PLATONA. L. Spek, *J. Appl. Crystallogr.* **2003**, *36*, 7–13.
- [23] K. Kambe, *J. Phys. Soc. Jpn.* **1950**, *5*, 48–51.

- [24] E. Aznar, S. Ferrer, J. Borrás, F. Lloret, M. Liu-Gonzalez, H. Rodriguez-Prieto, S. Garcia-Granda, *Eur. J. Inorg. Chem.* **2006**, 24, 5115–5125.
- [25] a) I. Dzyaloshinsky, *J. Phys. Chem. Solids* **1958**, 4, 241–255; b) T. Moriya, *Phys. Rev. Lett.* **1960**, 4, 228–230; T. Moriya, *Phys. Rev.* **1960**, 120, 91–98.
- [26] A. Ozarowski, Y. Shunzhong, B. R. McGarvey, A. Mislankar, J. E. Drake, *Inorg. Chem.* **1991**, 30, 3167–3174.
- [27] A. Bencini, D. Gatteschi in *EPR of Exchange Coupled Systems*, Springer Verlag, Berlin, Heidelberg **1990**.
- [28] V. V. Semenaka, O. V. Nesterova, V. N. Kokozay, V. V. Dyakonenko, R. I. Zubatyuk, O. V. Shishkin, R. Boca, J. Jezierska, A. Ozarowski, *Inorg. Chem.* **2010**, 49, 5460–5471.
- [29] J. H. Wilkinson in *The Algebraic Eigenvalue Problem*, Clarendon Press, London, **1970**.
- [30] R. Maurice, K. Sivalingam, D. Ganyushin, N. Guihéry, C. de Graaf, F. Neese, *Inorg. Chem.* **2011**, 50, 6229–6236.
- [31] P. K. Ross, M. D. Allendorf, E. I. Solomon, *J. Am. Chem. Soc.* **1989**, 111, 4009–4021.
- [32] a) D. L. Reger, A. Debreczeni, M. D. Smith, J. Jezierska, A. Ozarowski, *Inorg. Chem.* **2012**, 51, 1068–1083; b) A. Ozarowski, *Inorg. Chem.* **2008**, 47, 9760–9762.
- [33] F. Neese, *ORCA – an ab initio, Density Functional and Semiempirical Program Package*, Version 2.8, University of Bonn, **2008**. Free download from <http://www.thch.uni-bonn.de/tc/orca/> (registration required).
- [34] a) A. Schaefer, H. Horn, R. Ahlrichs, *J. Chem. Phys.* **1992**, 97, 2571–2577; b) the Ahlrichs auxiliary basis sets were obtained from the TurboMole basis set library under <ftp.chemie.uni-karlsruhe.de/pub/jbasen>; c) K. Eichkorn, O. Treutler, H. Ohm, M. Haser, R. Ahlrichs, *Chem. Phys. Lett.* **1995**, 240, 283–290; d) K. Eichkorn, F. Weigend, O. Treutler, R. Ahlrichs, *Theor. Chem. Acc.* **1997**, 97, 119–124.
- [35] a) D. A. Becke, *Phys. Rev. A* **1988**, 38, 3098–3100; b) J. P. Perdew, *Phys. Rev. B* **1986**, 33, 8822–8824; c) J. P. Perdew, *Phys. Rev. B* **1986**, 33, 8822–8824; J. P. Perdew, *Phys. Rev. B* **1986**, 34, 7406; d) R. A. Kendall, H. A. Früchtl, *Theor. Chem. Acc.* **1997**, 97, 158–163.
- [36] R. Prins, M. Biagini-Cingi, M. Drillon, R. A. G. de Graff, J. Haasnoot, A.-M. Manotti-Lanfredi, P. Rabu, J. Reedijk, F. Ugozzoli, *Inorg. Chim. Acta* **1996**, 248, 35–44.
- [37] P. J. van Koningsbruggen, J. W. van Hal, R. A. G. de Graaff, J. G. Haasnoot, J. Reedijk, *J. Chem. Soc., Dalton Trans.* **1993**, 2163–2167.
- [38] G. M. Sheldrick, *Acta Crystallogr., Sect. A* **2008**, 64, 112–122.
- [39] *Stoe & Cie. IPDS Software*, Stoe & Cie GmbH, Darmstadt, Germany, **2000**.
- [40] C. J. O'Connor, *Prog. Inorg. Chem.* **1982**, 29, 203–283.
- [41] G. A. Bain, J. F. Berry, *J. Chem. Educ.* **2008**, 85, 532–536.
- [42] A. K. Hassan, L. A. Pardi, J. Krzystek, A. Sienkiewicz, P. Goy, M. Rohrer, L.-C. Brunel, *J. Magn. Reson.* **2000**, 142, 300–312.

Received: July 30, 2012

Published Online: October 15, 2012